Elastic and inelastic scattering of pions from nuclei using an equivalent local potential

S. A. E. Khallaf and A. A. Ebrahim
Physics Department, Assiut University, Assiut 71516, Egypt
(Received 16 January 2002; published 23 May 2002)

Angular distributions for the elastic and inelastic scattering of pions by ^{40,42,44,48}Ca and ^{54}Fe at 116, 180, and 292.5 MeV have been analyzed. The equivalent local optical model calculations have been carried out for elastic and inelastic scattering of $\pi^{\pm}$ leading to the lowest 2^+ and 3^- states of these nuclei. Good reproductions of the data are obtained for these nuclei without adjusting any free parameters in the optical potential. Reaction cross sections and deformation lengths are consistent with other calculations of these quantities.

DOI: 10.1103/PhysRevC.65.064605 PACS number(s): 25.80.Dj, 25.80.Ek, 24.10.Eq, 27.40.+z

I. INTRODUCTION

The pion-nucleus scattering around 200 MeV is dominated by strong absorption arising from the resonance character of the pion-nucleon amplitude and the scattering is insensitive to the finer details of the pion-nucleus interaction. A number of analysis of differential, reaction, and total cross sections in the energy range 30–300 MeV have used the impulse approximation to construct an optical potential for pions in the limit of *s* and *p* waves only. These calculations show that this potential leads to a reasonable agreement with the data when used in a relativistic optical model code or in a semiclassical calculations [1].

Recently, elastic and inelastic scattering of positive and negative pions from calcium isotopes and ^{54}Fe were studied using Woods-Saxon (WS) local optical potentials together with a zero-range distorted-wave Born approximation code [2]. The elastic scattering studies resulted in considerable ambiguities in WS parameters. Using best fit parameters, calculations were carried out for inelastic scattering of pions of both signs to the lowest 2^+ and 3^- states of these targets, the corresponding deformation parameters were extracted and ambiguities in WS parameters were greatly reduced. It was concluded that the simple WS local potential model seems to be a useful one for pion-nucleus scattering without recourse to complexities of the nonlocal interactions.

On the other hand, in a previous work [3] the local potential of Johnson and Satchler [4] equivalent to Kisslinger nonlocal potential [5] was used to successfully analyze the elastic scattering of $\pi^{\pm}$ from ^{12}C, ^{16}O, ^{28}Si, and ^{40,44,48}Ca in the pion kinetic energy range of 30–292 MeV. The DWUCK4 code [6] was used to calculate the differential cross section angular distributions for elastically scattered pions. It was suggested to use the DWUCK4 code and equivalent local potential of Johnson and Satchler to compute the $\pi^{\pm}$ inelastic scattering cross sections from nuclei.

In the present work, the angular distributions of the differential cross sections of the $\pi^{\pm}$ elastically and inelastically scattered to the lowest 2^+ and 3^- states in ^{40,42,44,48}Ca and ^{54}Fe at 116, 180, and 292.5 MeV are calculated and compared to the experimental data [7]. The equivalent local potential of Johnson and Satchler is used without free parameters to fit the elastic scattering data and then this potential is used for the first time as far as we know to calculate the inelastic scattering angular distributions. The overall normalization of the inelastic cross sections give the deformation lengths. The deformation lengths are extracted and compared to those calculated using deformation and radius parameters of Ref. [2]. The method employed here is described in Sec. II, results and discussion are in Sec. III, and conclusions are in Sec. IV.

II. METHOD

We have used the local pion-nucleus optical potential of Johnson and Satchler [4] that is exactly equivalent to nonlocal potential of the Kisslinger form [5]. The equivalent local potential can be obtained by using the Krell-Ericson transformation, which converts the relativistic Klein-Gordon equation for pion scattering to the nonrelativistic Schrödinger equation. The transformed wave function ψ satisfies a Schrödinger equation,

$$\{-(\hbar^2/2\mu)\nabla^2 + U_L + V_C\}\psi = E_{\text{c.m.}}\psi. \tag{1}$$

U_L is the nuclear local transformed potential [4],

$$U_L(r) = U_N(r) + \Delta U_C(r), \tag{2}$$

where the Coulomb correction term $\Delta U_C(r)$ is [4]

$$\Delta U_C(r) = \frac{\alpha(r)V_C - (V_C^2/2\omega)}{1-\alpha(r)}, \tag{3}$$

and the nuclear local potential $U_N(r)$ is [4]

$$U_N(r) = \frac{(\hbar c)^2}{2\omega}\left\{\frac{q(r)}{1-\alpha(r)} - \frac{k^2\alpha(r)}{1-\alpha(r)} - \frac{\frac{1}{2}\nabla^2\alpha(r)}{1-\alpha(r)} - \left(\frac{\frac{1}{2}\nabla\alpha(r)}{1-\alpha(r)}\right)^2\right\}. \tag{4}$$

The quantity $q(r)$ mainly results from the *s*-wave part and $\alpha(r)$ results from the *p* wave part of the pion-nucleon interaction; $q(r)$ and $\alpha(r)$ can be expressed in terms of the target nuclei density distributions and their gradients. Both are complex and energy dependent and are given in detail in Ref. [4]. The pion-nucleon scattering amplitude depends on complex first-order and second-order interaction parameters. The

 ©2002 The American Physical Society

first-order interaction parameters are related to the free pion-nucleon scattering through the phase shifts in the form described in Ref. [8], and the phase shifts are calculated according to the recent relation of Ref. [9]. The second-order parameters are required only at lower energies $T_\pi \leqslant 80$ MeV, but these parameters make no differences in the calculations at higher energies, so they were set to be zero [3,9]. Here, V_C is the Coulomb potential due to the uniform charge distribution of the target nucleus of radius $R_C = r_C A^{1/3}$, A is the target mass number, and $r_C = 1.2$ fm [3].

The radial parts of the hadronic transition potential used here are as follows [10]:

$$V(r) = -\delta_l^N \frac{dU_L}{dr}, \tag{5}$$

where U_L is the local transformed potential found to fit the corresponding elastic scattering. For a given transition, we use δ_l^N with $N = \pm$ to denote the corresponding "deformation lengths" for the $\pi^\pm$ interaction, while $l(=2$ or $3)$ is the multipolarity.

The motivation here is to test the models of Eqs. (2) and (5) in this energy range for pion inelastic scattering. Success is expected because of the close relation between elastic and inelastic scattering to collective states in the presence of strong absorption [10].

III. RESULTS AND DISCUSSION

We have used the first-order equivalent local optical potential to analyze the elastic scattering of positive and negative pions with bombarding energies in the vicinity of the (3,3) resonance, 116–292.5 MeV, for ^{40,42,44,48}Ca and ^{54}Fe nuclei. The resulting kinematic parameter values for the cases studied here are calculated according to equations given in Ref. [10] and collected in Table I. The present equivalent local potential when deformed and applied to inelastic scattering data for the excitation of 2^+ and 3^- states is able to reproduce the experimental data. Here, we compare calculations based on the present equivalent local potential and those based on the Woods-Saxon local potential of Ref. [2] using the same kinematic parameters in both cases. All calculations use exactly the zero-range distorted wave Born approximation code DWUCK4 [6], except for that basic optical potential form. The present equivalent local optical potential calculations are shown as the solid curves and calculations using the WS local potential are shown as the dashed curves in Figs. 1–9.

For elastic and inelastic scattering from ^{40,42,44,48}Ca and ^{54}Fe, the values of the first-order parameters b_i and c_i $(i = 0,1)$ are of the same values for π^+ and π^- scattering at a certain beam energy. In the present calculations we used the three-parameter Fermi shape for the density distributions of nucleons within nuclei at the three considered energies with parameters taken from Table IV of Ref. [7] along with the Ericson-Ericson Lorentz-Lorentz (EELL) parameter $\zeta = 1.0$, they were more suitable for $\pi^\pm$-nucleus scattering using the equivalent local potential [3], in the same energy range considered here.

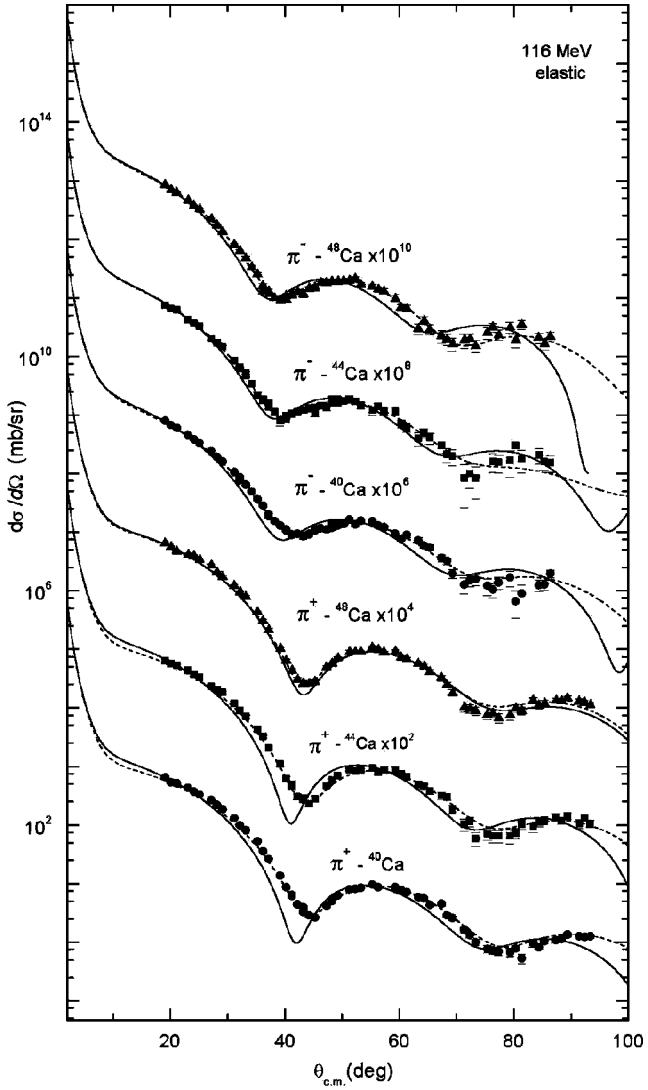

FIG. 1. Data for elastic scattering of 116-MeV $\pi^\pm$ from ^{40,44,48}Ca [7], compared with two curves computed with the present equivalent local potential as the solid curves and the WS calculations as the dashed curves.

Calculations of π^+ and π^- elastic scattering were carried out using the two forms of potentials at 116 MeV as shown in Fig. 1. The present calculations based on a first-order equivalent local potential with no adjustable parameters are shown as solid curves. Agreements between data [7] and calculations are good for all nuclei especially at forward angles, except for π^+-^{40,44}Ca cross sections at the first minimum which appear to be under data by about 15% and is shifted toward forward angles by about 3°. At large angles, the Woods-Saxon calculations are in better agreement with the data than the present local optical model calculations. This may be due to that the Woods-Saxon calculations were forced to agree with the data.

We show in Fig. 2 cross sections for pion elastic scattering computed on ^{40,42,44,48}Ca and ^{54}Fe at 180 MeV. Elastic cross sections computed with the two forms of potentials are identical, especially at forward angles and they are in good agreement with data [7].

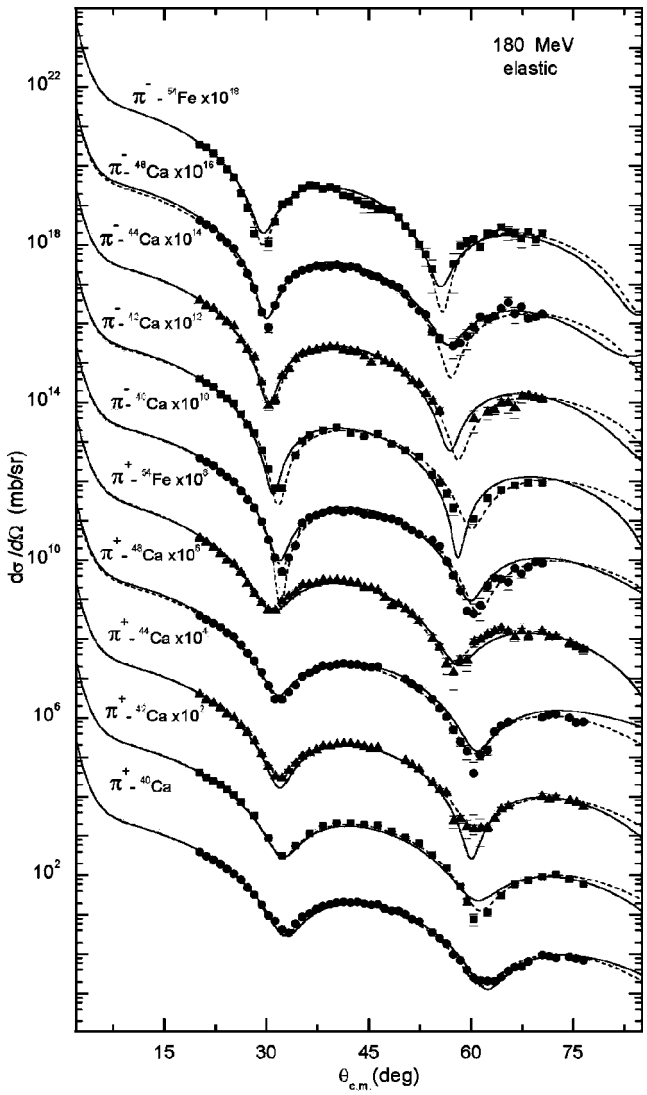

FIG. 2. As in Fig. 1 but for $\pi^{\pm}$-^{40,42,44,48}Ca and -^{54}Fe differential elastic cross sections at 180 MeV. The experimental data are taken from Ref. [7].

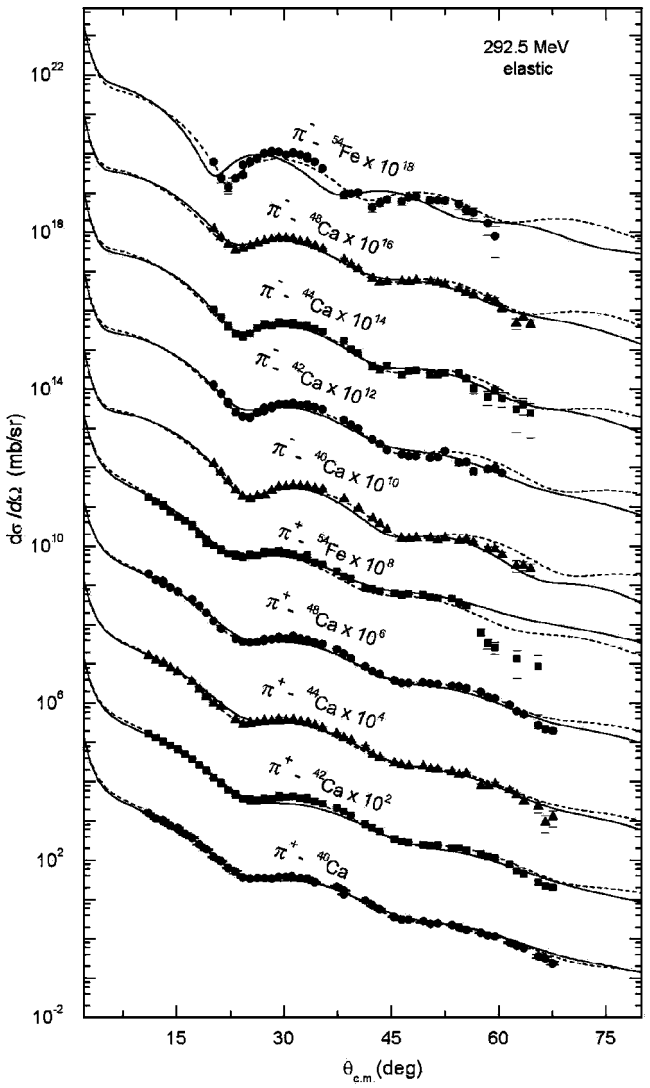

FIG. 3. As in Fig. 1 but for $\pi^{\pm}$-^{40,42,44,48}Ca and -^{54}Fe differential elastic cross sections at 292.5 MeV. The experimental data are taken from Ref. [7].

At 292.5 MeV, where more partial waves up to $l_{\max}=20$ are required, the elastic scattering with both pion signs are calculated using the present first-order local potential and compared to data [7] and calculations based on the WS local potential of Ref. [2], as shown in Fig. 3. The two equivalent local and Woods-Saxon potential calculations are very close, except for π^- scattered from ^{54}Fe, the WS local potential gives a better fit with data than do the present calculations.

Inelastic scattering is another important aspect of the interactions of pions with nuclei. In a phenomenological approach, it is expected that both elastic and inelastic scattering will be described in the same framework. This consistency may provide more information on the pion-nucleus potential and is essential before reliable nuclear structure information can be expected.

With the zero-range distorted-wave Born approximation, we may also compute inelastic scattering to the collective 2^+ and 3^- states of the targets ^{40,42,44,48}Ca and ^{54}Fe by using the standard light ion code DWUCK4 [6]. When the first-order local potential is deformed, the value of the deformation length δ_l^N is to be adjusted to obtain a reasonable agreement with the data and can be found as shown in Figs. 4–9. Coulomb excitation is found to be unimportant for the inelastic scattering cases considered here. The resulting deformation lengths determined by visually adjusting the calculations to reproduce the equivalent data are listed in Tables I and II compared to those obtained from calculations using parameters given in Table 2 of Ref. [2]. To calculate deformation lengths from parameters of Ref. [2], we used the relations

$$\delta_{\text{real}}^{\pm}=\beta_l^{\pm} r_u A^{1/3},$$

$$\delta_{\text{imag.}}^{\pm}=\beta_1^{\pm} r_w A^{1/3}, \tag{6}$$

where $\beta_l^{\pm}$, r_u, and r_w are defined and given in Ref. [2].

The angular distributions for the inelastic scattering of $\pi^{\pm}$ by ^{44}Ca (2^+; 1.16 MeV) and ^{48}Ca (2^+; 3.83 MeV) at 116 MeV pion kinetic energy are presented in Fig. 4. Rather

TABLE I. Interaction parameter values used in present work for pions with pion kinetic energy T_π. k, p_1, E_L, and M_π are the pion wave number, kinematic transformation factor, effective bombarding energy, and effective pion mass, respectively.

T_π (MeV)	Target	k (fm^{-1})	p_1	E_L (MeV)	M_π (μ)
116	^{40}Ca	1.0789	1.2649	89.9077	0.2728
	^{42}Ca	1.0791	1.2653	89.8877	0.2729
	^{44}Ca	1.0795	1.2658	89.8695	0.27292
	^{48}Ca	1.080	1.2665	89.8376	0.2731
180	^{40}Ca	1.4459	1.2329	129.916	0.3403
	^{42}Ca	1.4465	1.3305	129.875	0.3404
	^{44}Ca	1.4471	1.3311	129.837	0.3405
	^{48}Ca	1.4479	1.3321	129.771	0.3407
	^{54}Fe	1.4491	1.3334	129.69	0.3409
292.5	^{40}Ca	2.0502	1.4429	195.047	0.4583
	^{42}Ca	2.0512	1.4439	194.955	0.4586
	^{44}Ca	2.0523	1.4449	194.872	0.4589
	^{48}Ca	2.0541	1.4465	194.725	0.4591
	^{54}Fe	2.0562	1.4484	194.545	0.4596

TABLE II. Deformation lengths from π^+ inelastic scattering compared to those calculated using the parameters of Ref. [2] as discussed in the text. Note that in each case the upper number is the deformation length from the present work and the lower is the deformation length using the parameters of Ref. [2].

		2^+			3^-		
T_π (MeV)	Target	E_{ex} (MeV)	$\delta^+_{2)real}$ (fm)	$\delta^+_{2)imag.}$ (fm)	E_{ex} (MeV)	$\delta^+_{3)real}$ (fm)	$\delta^+_{3)imag.}$ (fm)
116	^{40}Ca				3.74	1.295	0.921
						1.344	0.896
	^{44}Ca	1.16	1.457	0.725	3.31	0.925	0.589
			1.324	0.883		0.884	0.590
	^{48}Ca	3.83	0.715	0.474	4.51	0.915	0.375
			0.641	0.436		0.732	0.498
180	^{40}Ca				3.74	1.75	1.300
						1.873	1.316
	^{42}Ca	1.52	1.512	0.985	3.45	1.579	1.052
			1.417	0.976		1.615	1.142
	^{44}Ca	1.16	1.488	1.105	3.31	1.356	0.919
			1.453	0.988		1.287	0.876
	^{48}Ca	3.83	1.185	0.615	4.51	1.625	0.725
			1.015	0.691		1.389	0.945
	^{54}Fe	1.410	1.056	0.718	4.78	0.650	0.385
			1.060	0.739		0.661	0.463
292.5	^{40}Ca				3.74	2.025	1.125
						1.921	1.284
	^{42}Ca	1.52	1.508	0.964	3.45	1.597	1.031
			1.416	0.913		1.620	1.044
	^{44}Ca	1.16	1.417	0.942	3.31	1.108	0.634
			1.429	1.022		1.077	0.770
	^{48}Ca	3.83	1.122	0.721	4.51	1.235	0.776
			0.901	0.634		1.183	0.832
	^{54}Fe	1.41	1.209	0.775	4.78	0.699	0.483
			1.225	0.824		0.729	0.490

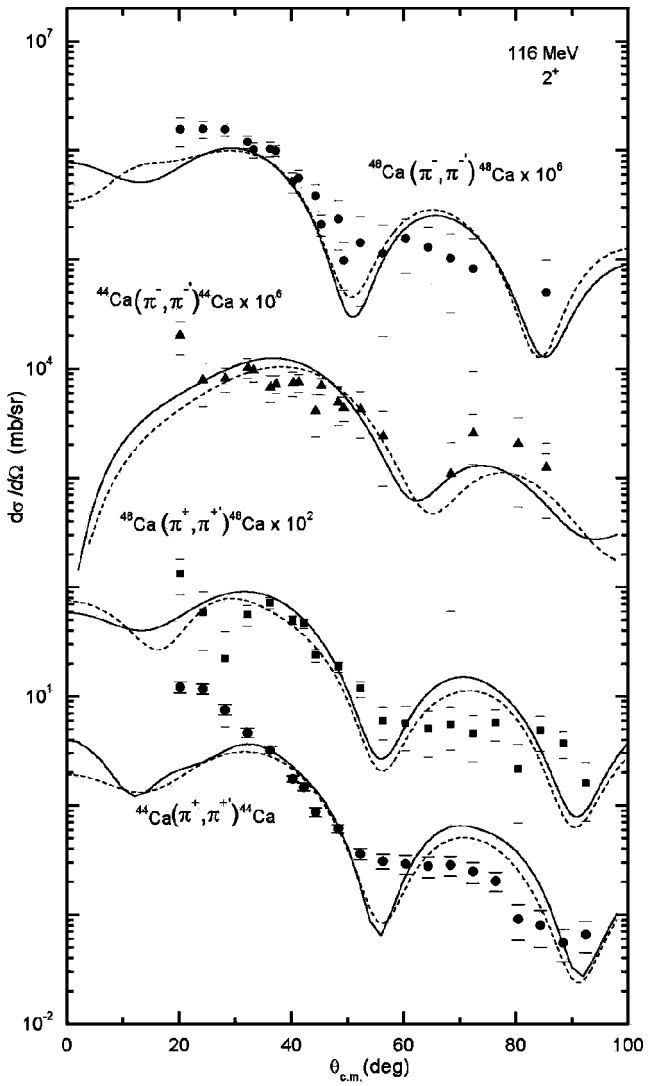

FIG. 4. Inelastic $\pi^{\pm}$ data [7] at 116 MeV exciting the 1.16-MeV 2^+ state of ^{44}Ca and 3.38-MeV 2^+ state of ^{48}Ca are compared with two curves computed with the present equivalent local potential as the solid curves and the WS calculations as the dashed curves.

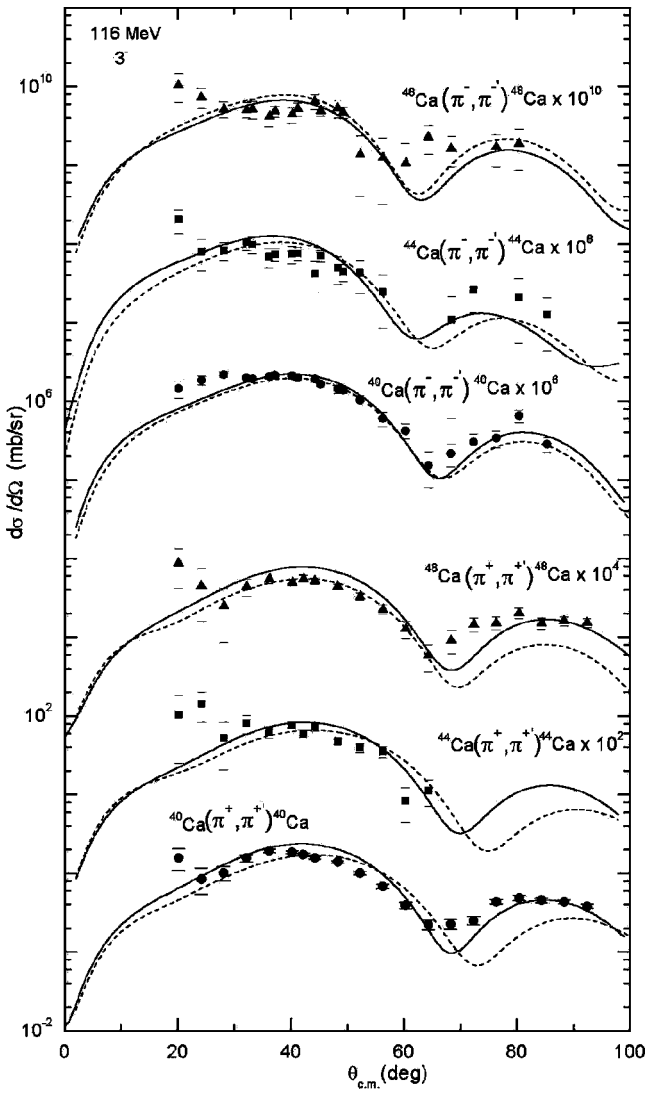

FIG. 5. As in Fig. 4 but for $\pi^{\pm}$-^{40,44,48}Ca differential inelastic cross sections at 116-MeV exciting the 3.74-MeV 3^- state of ^{40}Ca, 3.31-MeV 3^- state of ^{44}Ca, and 4.51-MeV 3^- state of ^{48}Ca. The experimental data are taken from Ref. [7].

poorer agreement is obtained for calculations of π^+ scattering to the 2^+ state in ^{44}Ca and ^{48}Ca, although the general shapes of the angular distributions are well reproduced by the present calculations.

Angular distributions for the inelastic scattering of $\pi^{\pm}$ by ^{40}Ca (3^-; 3.74 MeV), ^{44}Ca (3^-; 3.31 MeV), and ^{48}Ca (3^-; 4.51 MeV) at 116 MeV pion kinetic energy are presented in Fig. 5. The experimental angular distributions displayed in Fig. 5 are generally smooth, without well-defined minima. The $\pi^{\pm}$ angular distributions using either set of π-nucleus potential are similar in all cases except for π^+-^{40,44}Ca, where a shift in the locations of the minima is observed. This shift is comparable to that seen in the elastic scattering calculations.

The inelastic scattering of π^+ and π^- has been calculated at 180 MeV. The two sets of π-nucleus potential provide a reasonable description of data of $\pi^{\pm}$ inelastic scattering on ^{40,42,44,48}Ca and ^{54}Fe to the lowest 2^+ and 3^- states, as shown in Figs. 6 and 7.

For the data at 292.5 MeV shown in Figs. 8 and 9, angular distributions of the inelastic scattering of $\pi^{\pm}$ to the 2^+ state on ^{48}Ca and to 3^- state on ^{40,48}Ca, except for π^- scattering to the 2^+ state on ^{48}Ca, inelastic scattering calculations with the present local optical potential do somewhat better in describing the shapes of the inelastic angular distributions than do the WS calculations to the measured inelastic scattering data [7].

From Tables II and III, it can be seen that values of deformation lengths determined here using the equivalent local potential are very similar to those obtained from parameters of Ref. [2]. Most of the deformation lengths extracted from π^+ inelastic scattering on the considered nuclei are of negligible difference from those for π^- scattering. In case of ^{48}Ca at 180 MeV the noticeable differences between π^+ and π^- deformation lengths may be attributed to the fit shown in Fig. 5 of calculations with the experimental data.

Our first-order equivalent local potential is also used to

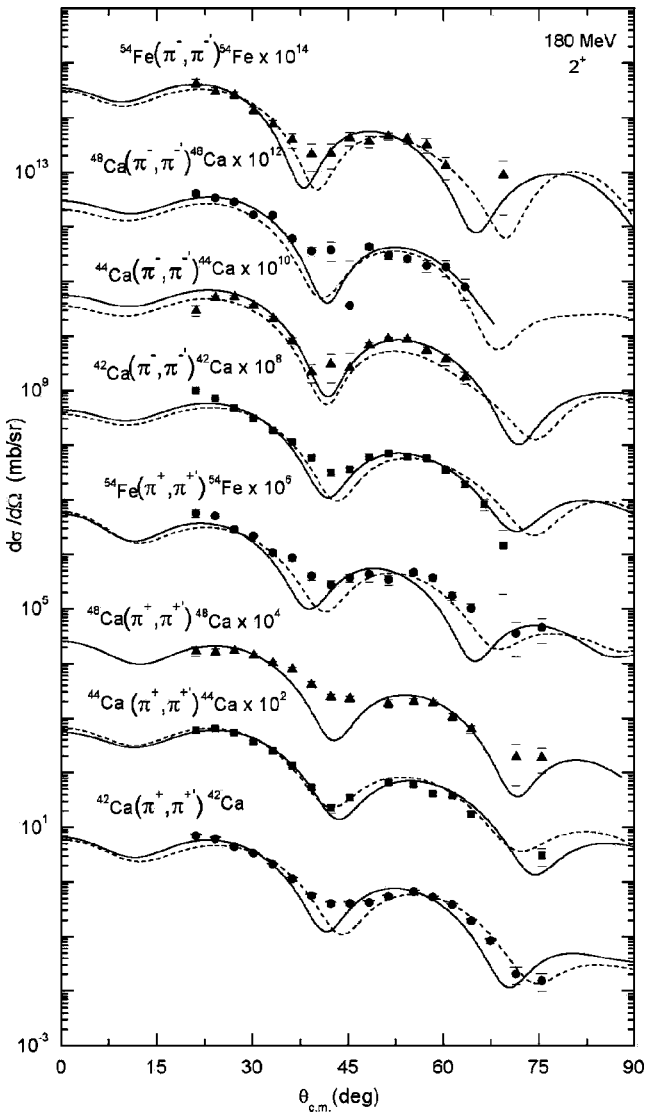

FIG. 6. As in Fig. 5, but for $\pi^{\pm}$-^{42,44,48}Ca and -^{54}Fe differential inelastic cross sections at 180-MeV 2^+ states of these nuclei. The experimental data are taken from Ref. [7].

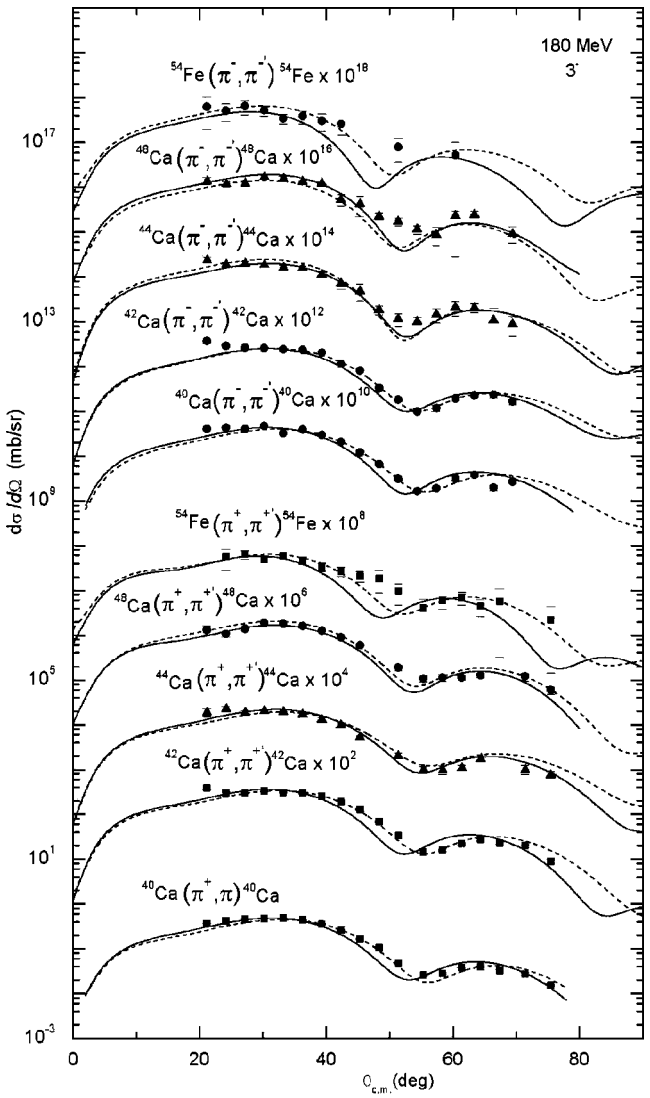

FIG. 7. As in Fig. 5, but for $\pi^{\pm}$-^{40,42,44,48}Ca and -^{54}Fe differential inelastic cross sections at 180-MeV to the lowest 3^- states of these nuclei. The experimental data are taken from Ref. [7].

predict reaction cross sections σ_R of both pion signs scattering on ^{40,42,44,48}Ca and ^{54}Fe at 116, 180, and 292.5 MeV; the DWUCK4 program [6] used here calculates these cross sections. The comparisons between our computations and those of Ref. [2] are listed in Table IV. It can be seen from Table IV that there is a very good agreement between the present calculations of σ_R for pions of both signs and those of Ref. [2]. This indicates that the imaginary part of the equivalent optical potential used here, which is strongly correlated to σ_R, is well predicted. There are strong absorption of positive pions at the resonance region confirmed by higher values of σ_R while this absorption of positive pions is weaker at lower and higher incident pion energies. Table IV also displays the total cross sections σ_T for $\pi^{\pm}$ predicted by the DWUCK4 code for the present reactions using the equivalent local potential. Since the pion mean free path λ is proportional to the inverse of the total π-nucleon cross sections, i.e., $\lambda \propto 1/(\sigma_T/A)$ [11], it is easy to see from Table IV that λ for π^+ is shorter in the resonance region than in higher and lower regions. This confirms that the positive pions are strongly absorbed at the surface of target nuclei. From Table IV it is noticed for π^- scattering from a certain nucleus that both calculated σ_T and σ_R decrease as the beam energy increases and values of σ_T for π^- for all considered nuclei at the three energies, except for ^{54}Fe at 292.5 MeV, are greater than those for π^+. This indicates that λ for π^- is shorter than the corresponding λ for π^+. It is also noticed that for pions of both signs, at a certain energy, σ_T and σ_R increase as mass number of target nucleus increases except the case of ^{48}Ca at 116 MeV.

IV. CONCLUSION

The conclusion reached from these large calculations is that the use of a local optical potential equivalent to the Kisslinger one without free parameters predicts well the cross sections of $\pi^{\pm}$ elastic and inelastic scattering. The calculations have the same validity using either the present first-

TABLE III. As in Table II but for π^- inelastic scattering. Note that in each case the upper number is the deformation length from the present work and the lower is the deformation length using the parameters of Ref. [2].

		2^+			3^-		
T_π (MeV)	Target	E_{ex} (MeV)	$\delta^-_{2)real}$ (fm)	$\delta^-_{2)imag.}$ (fm)	E_{ex} (MeV)	$\delta^-_{3)real}$ (fm)	$\delta^-_{3)imag.}$ (fm)
116	^{40}Ca				3.74	1.500	0.915
						1.361	0.960
	^{44}Ca	1.16	1.356	0.975	3.31	0.925	0.589
			1.350	1.006		0.934	0.696
	^{48}Ca	3.83	0.915	0.425	4.51	0.785	0.355
			0.801	0.583		0.903	0.657
180	^{40}Ca				3.74	1.920	1.200
						1.719	1.228
	^{42}Ca	1.52	1.416	0.998	3.45	1.219	0.935
			1.363	0.973		1.358	0.970
	^{44}Ca	1.16	1.488	1.105	3.31	1.056	0.815
			1.333	0.918		1.349	0.929
	^{48}Ca	3.83	1.375	0.775	4.51	1.383	0.785
			1.361	0.907		1.247	0.832
	^{54}Fe	1.41	1.070	0.733	4.78	0.625	0.325
			1.071	0.733		0.653	0.447
292.5	^{40}Ca				3.74	2.135	1.155
						1.987	1.305
	^{42}Ca	1.52	1.475	0.935	3.45	1.427	1.012
			1.491	0.994		1.503	1.002
	^{44}Ca	1.16	1.538	1.117	3.31	1.203	0.820
			1.699	1.136		1.660	0.799
	^{48}Ca	3.83	1.173	0.692	4.51	1.105	0.576
			1.056	0.717		1.001	0.679
	^{54}Fe	1.41	1.108	0.787	4.78	0.663	0.495
			1.141	0.877		0.673	0.517

TABLE IV. Total and reaction cross sections in mb for $\pi^\pm$ scattering on the considered nuclei calculated in the present work compared to those of [2].

		π^+			π^-		
	Target	This calculation		From [2]	This calculation		From [2]
T_π		σ_T	σ_R	σ_R	σ_T	σ_R	σ_R
116	^{40}Ca	1336.1	796.44	788	1553.1	934.6	916.8
	^{44}Ca	1370.1	828.2	821.5	1746.0	1047.4	1041.6
	^{48}Ca	1394.5	837.7	836.7	1744.0	1038.4	1028.0
180	^{40}Ca	1413.8	860.0	839.6	1484.4	903.3	900.4
	^{42}Ca	1431.6	870.0	852.9	1533.4	932.6	931.9
	^{44}Ca	1464.8	895.7	887.9	1621.3	978.2	982.5
	^{48}Ca	1471.0	891.9	870.5	1694.8	1017.0	1009.6
	^{54}Fe	1613.7	972.9	952.8	1759.3	1053.9	1046.1
292.5	^{40}Ca	1234.3	719.5	723.9	1244.5	703.9	701.5
	^{42}Ca	1281.2	741.6	742.2	12946	724.5	718.9
	^{44}Ca	1280.7	765.7	763.2	1377.1	765.5	757.5
	^{48}Ca	1303.1	752.95	749.2	1456.0	766.4	760.3
	^{54}Fe	1515.6	852.8	863.1	1491.3	792.6	793.1

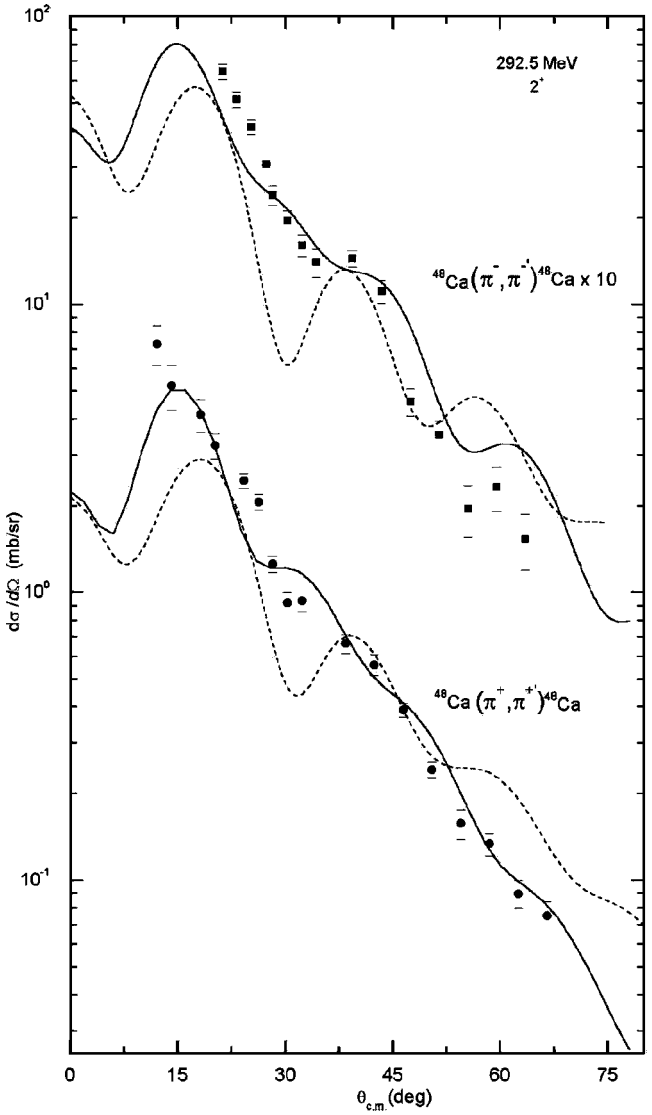

FIG. 8. As in Fig. 5, but for $\pi^{\pm}$-^{48}Ca differential inelastic cross sections at 292.5 MeV to the lowest 2^+ state of ^{48}Ca. The experimental data are taken from Ref. [7].

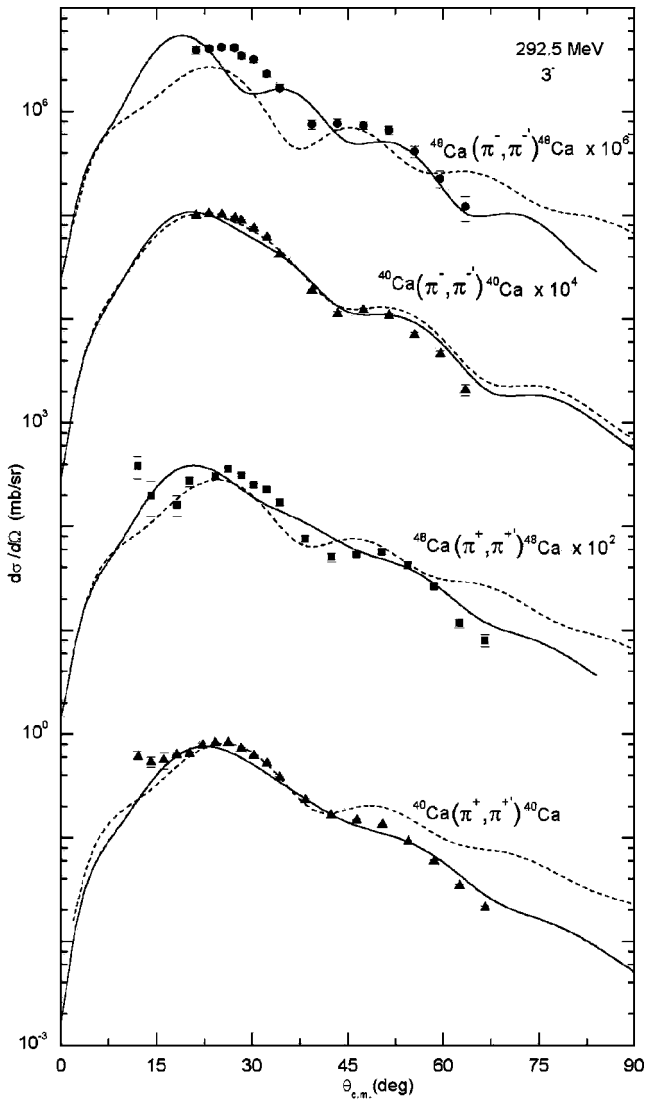

FIG. 9. As in Fig. 5, but for $\pi^{\pm}$-^{40,48}Ca differential inelastic cross sections at 292.5 MeV to the lowest 3^- states of these nuclei. The experimental data are taken from Ref. [7].

order local optical potential or the Woods-Saxon local optical potential forms for π-nucleus potential with zero-range DWUCK4 code. The resulting inelastic angular distributions of the present local optical potential have both shapes and magnitudes consistent with data [7]. Differences between the present local potential and the WS potential are very small when they are used to compute elastic and inelastic scattering of pions from nuclei.

The short mean free path of the pion in the Δ region produces pronounced Fraunhofer diffraction patterns in the elastic scattering from nuclei. This appears clearly from Fig. 2. Outside the resonance region the diffractive character of the angular distributions is still apparent but less pronounced (see Figs. 1 and 3). In particular, the minima are systematically more shallow both above and below the resonance.

Finally, we can suggest the use of the present local potential in pion charge exchange calculations.

[1] P. E. Hodgson, *Nuclear Reactions and Nuclear Structure* (Oxford University Press, New York, 1971).

[2] Md. A. E. Akhter, Sadia Afroze Sultanaa, H. M. Sen Gupta, and R. J. Peterson, J. Phys. G **27**, 755 (2001).

[3] S. A. E. Khallaf and A. A. Ebrahim, Phys. Rev. C **62**, 024603 (2000).

[4] M. B. Johnson and G. R. Satchler, Ann. Phys. (N.Y.) **248**, 134 (1996).

[5] L. S. Kisslinger, Phys. Rev. **98**, 761 (1955).

[6] P. D. Kunz, computer code DWUCK4, University of Colorado; P. D. Kunz and E. Rost, in *Nuclear Reactions*, Vol. 2 of Computational Nuclear Physics, edited by K. Langanke, J. A. Maruhn,

and S. E. Koonin (Springer-Verlag, New York, 1993).
[7] K. G. Boyer *et al.*, Phys. Rev. C **29**, 182 (1984).
[8] J. Bartel, M. B. Johnson, and M. K. Singham, Ann. Phys. (N.Y.) **196**, 89 (1989); S. J. Greene *et al.*, Phys. Rev. C **30**, 2003 (1984); R. A. Gilman, Ph.D. dissertation, University of Pennsylvania, 1985.
[9] A. A. Ebrahim and R. J. Peterson, Phys. Rev. C **54**, 2499 (1996).
[10] G. R. Satchler, Nucl. Phys. **A540**, 533 (1992).
[11] C. B. Dover and G. E. Walker, Phys. Rep. **89**, 1 (1982).